Journal of ELECTRONIC MATERIALS, Vol. 45, No. 7, 2016
DOI: 10.1007/s11664-016-4536-z
© 2016 The Minerals, Metals & Materials Society

CrossMark

Characterization of AlInN/AlN/GaN Heterostructures with Different AlN Buffer Thickness

S. ÇÖREKÇİ,[1,5] S. DUGAN,[2] M.K. ÖZTÜRK,[3] S.Ş. ÇETİN,[3] M. ÇAKMAK,[3] S. ÖZÇELİK,[3] and E. ÖZBAY[4]

1.—Energy Systems Engineering Department, Kırklareli University, 39000 Kırklareli, Turkey. 2.—Physics Department, Kırklareli University, 39000 Kırklareli, Turkey. 3.—Photonics Research Center, Gazi University, 06500 Ankara, Turkey. 4.—Nanotechnology Research Center, Bilkent University, 06800 Ankara, Turkey. 5.—e-mail: scorekci@klu.edu.tr

Two AlInN/AlN/GaN heterostructures with 280-nm- and 400-nm-thick AlN buffer grown on sapphire substrates by metal-organic chemical vapor deposition (MOCVD) have been investigated by x-ray diffraction (XRD), atomic force microscopy (AFM), photoluminescence (PL) and Hall-effect measurements. The symmetric (0002) plane with respect to the asymmetric $(10\bar{1}2)$ plane in the 280-nm-thick AlN buffer has a higher crystal quality, as opposed to the 400-nm-thick buffer. The thinner buffer improves the crystallinity of both (0002) and $(10\bar{1}2)$ planes in the GaN layers, it also provides a sizeable reduction in dislocation density of GaN. Furthermore, the lower buffer thickness leads to a good quality surface with an rms roughness of 0.30 nm and a dark spot density of $4.0 \times 10^8\ cm^{-2}$. The optical and transport properties of the AlInN/AlN/GaN structure with the relatively thin buffer are compatible with the enhancement in its structural quality, as verified by XRD and AFM results.

Key words: AlInN/AlN/GaN HEMT, AlInN barrier, AlN buffer

INTRODUCTION

III-nitride (III-N) based high-electron-mobility transistors (HEMTs) have emerged as strong candidates for high-power and high-frequency applications, due to the large breakdown field and excellent electron transport properties.[1,2] The layered nitride structures on foreign substrates such as sapphire, silicon carbide or silicon have been used to realize HEMTs. The performance of HEMT devices depends on the structural quality and the layer design of III-N heterostructure. Extensive research efforts on the heterostructure configuration have been made to improve the transport properties in the past few decades. As is well known, Al concentration in AlGaN barrier layer of a conventional AlGaN/GaN heterojunction is an important design parameter. In such a structure, an increasing Al composition enhances the barrier height, and the carrier density increases as a result of better confinement of carriers in the channel.[3] However, the increased Al percentage (≥30%) degrades the crystalline quality of the ternary barrier by leading a high defect density because of lattice mismatch between AlGaN and GaN, and hence the carrier mobility reduces significantly.[4–6] Another way to improve the transport properties is the introduction of a very thin (1 nm) AlN layer between AlGaN barrier and GaN main layers in the conventional structure. The AlN interlayer increases the electron mobility by eliminating the alloy disorder scattering in AlGaN/GaN heterostructure and the carrier density by enhancing barrier height.[7]

On the other hand, Kuzmík revealed that the use of an AlInN/GaN heterostructure with AlInN barrier layer would improve the performance of HEMTs.[8] AlInN is lattice-matched (LM) to GaN at an In composition of approximately 17%, and thereby the limitations from the strain in AlGaN/GaN based structures can be eliminated by the novel LM-configuration and the structural defects in the heterostructure can be reduced.[8–10] Furthermore, the LM-system possesses a higher carrier

(Received December 17, 2015; accepted April 11, 2016; published online May 3, 2016)

density than the standard design because of the stronger spontaneous polarization effect and the larger conduction band offset.[8,10,11] For these reasons, AlInN/GaN heterostructures have recently attracted considerable interest.[11–14] In addition to above-stated structure, the growth of an InGaN back barrier on the thick-GaN buffer layer is a promising approach that improves the pinch-off quality of the devices owing to the better confinement of the electrons in the channel.[15]

The novel AlInN-HEMT configuration has a high potential for improving the performance of device. However, the growth of a high-crystal-quality AlInN barrier is a great challenge on account of the different optimum growth temperatures for AlN (∼1100°C) and InN (∼600°C) in MOCVD, and the large difference bonding energy between Al-N (2.88 eV) and In-N (1.98 eV).[5,16,17] The threading dislocation (TD) densities in III-N layers grown on sapphire is at a level of between 10^7 cm^{-2} and 10^{11} cm^{-2}. The electrical properties of the defects have been extensively studied by several research groups.[5,18] Despite all these difficulties, the good-quality AlInN layers have been achieved on AlN templates at low pressure by Sakai et al.[17] In one of our former studies,[19] we demonstrated that AlN templates on sapphire improved the crystalline quality and morphology of the AlGaN/GaN structures. Consequently, the AlN templates are of crucial importance in terms of transistor performance and their effects are needed to determine for further improvement of the these new structures. Here we present the effects of buffer thickness on the crystallinity, morphology, optical and electrical properties of AlInN/AlN/GaN heterostructures.

GaN cap (2 nm)
AlInN barrier (10 nm)
AlN interlayer (~1-2 nm)
GaN (2 nm)
InGaN back barrier (20 nm)
GaN buffer (140 nm)
GaN buffer (280 nm)
ud-GaN (810 nm)
ud-GaN (180 nm)
AlN buffer
(280 nm for sample A)
(400 nm for sample B)
AlN nucleation
sapphire substrate

Fig. 1. Schematic cross-sectional view of layer structure of the samples.

EXPERIMENTS

The HEMT samples discussed in this work were grown on *c*-plane sapphire substrates using AlN as a buffer layer by MOCVD system, in an AIX 200/4 RF-S reactor. Trimethylindium, trimethylgallium, trimethylaluminum, and high-purity ammonia were used as In, Ga, Al and N precursors. Two types of structures were prepared by using the buffer layers in nominal thicknesses of 280 nm and 400 nm with the aim of determine the effects on the layers of buffer thickness (hereinafter, they will be referred to as samples A and B). The side view of them is shown schematically in Fig. 1. The growth was initiated with the deposition of AlN nucleation at a temperature of 770°C and at a pressure of 50 mbar. Next, the reactor temperature was raised to 1150°C and AlN buffer growth was conducted under a pressure of 35 mbar. After the AlN growth, undoped (ud) GaN layers, GaN buffer layers, an InGaN back-barrier layer, a thin GaN layer, an AlN interlayer, an AlInN barrier layer and a GaN cap layer were deposited. The growth conditions of these layers in both samples were kept constant except for growth temperature of the back barrier. In percentages for the AlInN barriers were also kept constant to compare the properties of the samples, independent of the In content. The structural characterization was carried out by x-ray diffraction (XRD) and atomic force microscopy (AFM). The XRD measurements of the samples were performed on a Bruker D8-Discover instrument. The AFM surface images of the cap layers were collected by using an Omicron VT-STM/AFM instrument. The optical properties of the structures were analyzed by photoluminescence (PL) measurements at room temperature. The PL spectra for the samples were recorded on a Horiba Jobin–Yvon Florog-550 photoluminescence system with a 325 nm line of a 50 mW He–Cd laser. The room-temperature electron mobility and the sheet carrier density of the heterostructures were determined by Hall-effect measurements. For these measurements, square shaped samples with four evaporated Ti/Al/Ni/Au Ohmic contacts in the corners were prepared. The electrical contacts were made by using gold wires and In soldering, and their Ohmic behavior was verified by the current-voltage characteristics.

RESULTS AND DISCUSSION

Crystallinity of the layers in the heterostructure is very important in terms of HEMT performance. XRD is a non-destructive method in analyzing the structure of epitaxial films. Crystalline quality of

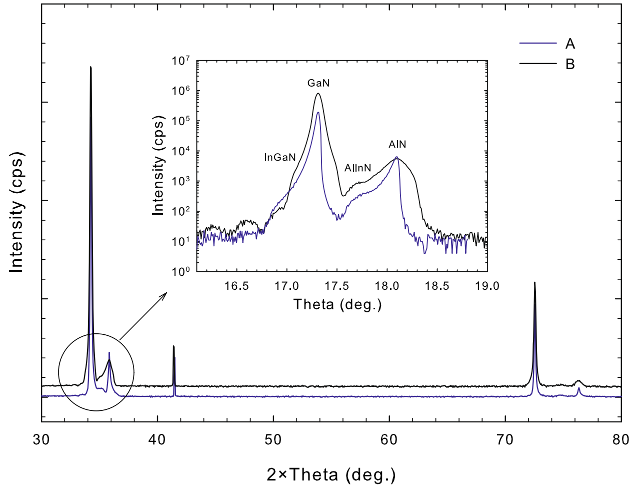

Fig. 2. (Color online) Typical XRD $\omega - 2\theta$ scans of the samples. The inset shows Bragg reflections from the (0002) crystal planes of layers in the structures.

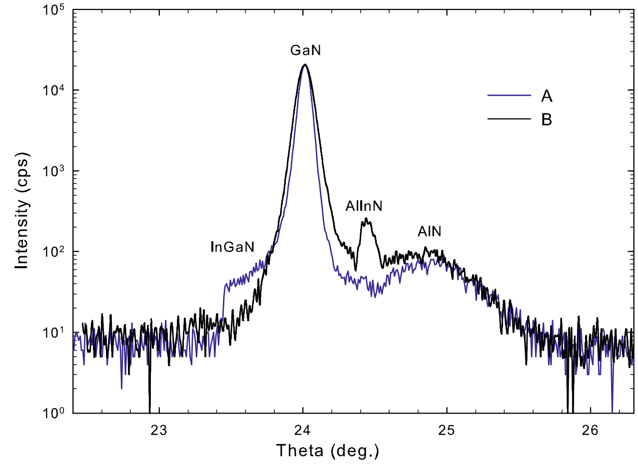

Fig. 3. (Color online) $(10\bar{1}2)$ Bragg reflections for two samples with 280- and 400-nm-thick AlN buffer grown on sapphire substrates.

the layers in the samples was evaluated utilizing symmetric (0002) and asymmetric $(10\bar{1}2)$ x-ray scans. Figure 2 displays XRD patterns of samples A and B, which exhibit strong diffraction peaks corresponding to the nominal structures shown in Fig. 1. The inset shows the (0002) reflections from the epitaxial layers of both samples. The AlInN(0002) peaks are clearly observed for both samples. Figure 3 contains the $(10\bar{1}2)$ reflections from the samples, which their narrowness represents the high crystalline quality of the asymmetric planes in the layers. The full-width at half-maximums (FWHMs) of AlN (0002) and AlN $(10\bar{1}2)$ peaks were determined as 0.067°, 0.376° for sample A and 0.260°, 0.243° for sample B, as tabulated in Table I. The increase in layer thickness has an opposite effect on the symmetric and asymmetric peaks of AlN as seen from these values. While the symmetric peaks broaden with the increasing thickness, the asymmetric peaks narrow. In other words, the increase in thickness of the layer improves crystallinity of $(10\bar{1}2)$ plane in the AlN, and degrades that of the (0002) one. This is very well in agreement with our report[20] showing that thicker layer growth is effective in improving the quality of the $(10\bar{1}2)$ plane in AlN film.

The presence of a large amount of the TDs in III-N layers is one of the main factors limiting the performance of HEMT devices because they are scattering centers for the carriers. The TDs are of three types; pure screw with Burgers vector $b = \langle 0001 \rangle$ pure edge with Burgers vector $b = \frac{1}{3}\langle 11\bar{2}0 \rangle$ and mixed with Burgers vector $b = \frac{1}{3}\langle 11\bar{2}3 \rangle$. The (0002) peak is broadened by screw component TDs in an epilayer, whereas the $(10\bar{1}2)$ one is broadened via all the TDs.[21] In accordance with the FWHMs of AlN, it is obvious that the vast majority of TDs in sample A are the edge component of dislocation. This is a typical feature for MOCVD-grown AlN films and similar to the previously reported results.[20,21] Additionally, the thicker buffer layer in sample B in comparison to sample A has a higher screw dislocation density. As a consequence of increased thickness, the degrading effect on the crystallinity of the (0002) plane is more pronounced than the improving effect on the $(10\bar{1}2)$ plane. According to the report of Faleev et al.,[22] in case of increase of layer thickness, the point defects in GaN begin to transform into the screw TDs owing to the diminution of elastic strain in the accommodation sublayer. In this frame, the structural transformation of crystal defects may lead to a rise in density of screw-type dislocations for AlN in sample B. The FWHMs of GaN (0002), GaN $(10\bar{1}2)$ and AlInN (0002), AlInN $(10\bar{1}2)$ peaks are obtained as 0.044°, 0.078° and 0.221°, 0.250° for sample A and 0.074°, 0.104° and 0.234°, 0.243° for sample B (Table I). As these values are compared, it can be seen that the GaN layer having a broader peak grown on 400-nm-thick buffer (in sample B) has poorer crystalline quality than the layer on 280-nm-thick buffer (in sample A). In other words, a relatively thicker buffer layer on sapphire degrades the quality of GaN layer. However, there is no significant change in the crystallinity of AlInN barriers in the samples because of the buffer thickness. Heteroepitaxially grown nitride layers in consequence of the large mismatch unavoidably brings a high defect density up to 10^{10} cm^{-2}, particularly dislocation density. The defect densities of heavily dislocated layers can be determined by performing the FWHMs of peaks. The dislocation densities in GaN for the samples are estimated by following expressions[23,24]:

$$D_S = \frac{\beta^2_{(0002)}}{9b^2_S},\ D_E = \frac{\beta^2_{(10\bar{1}2)}}{9b^2_E} \quad (1)$$

Table I. The dislocation density, dark spot density, rms roughness and FWHM values for the samples

	Layers	Sample A	Sample B
Edge dislocation density (cm^{-2})	GaN	2.0×10^8	3.6×10^8
Screw dislocation density (cm^{-2})	GaN	2.4×10^7	6.9×10^7
Dark spot density (cm^{-2})	GaN cap	4.0×10^8	8.3×10^8
rms roughness (nm)	GaN cap	0.30	0.46
(0002) FWHM (°)	AlN	0.067	0.260
	GaN	0.044	0.074
	AlInN	0.221	0.234
$(10\bar{1}2)$FWHM(°)	AlN	0.376	0.243
	GaN	0.078	0,104
	AlInN	0.250	0.243

where D_S and D_E are the screw-type and edge-type dislocation densities, β is the FWHM of GaN peak in Figs. 3 and 4, b is the Burgers vector length ($b_S = 0.5185$ nm, $b_E = 0.3189$ nm). As tabulated in Table I, the screw and edge dislocation densities of GaN were calculated as 2.4×10^7 cm^{-2}, 2.0×10^8 cm^{-2} for sample A and 6.9×10^7 cm^{-2}, 3.6×10^8 cm^{-2} for sample B, which are comparable to that of good-quality GaN epilayers. As was to be expected, the density of screw component is smaller by up to approximately one order of magnitude than that of the edge component or GaN predominantly includes edge type of TDs. Transmission electron microscopy observations of GaN/sapphire structure revealed that the TDs with screw component originate from the stacking disorder in the initial layer.[21] According to this, it can be concluded that sample B has a region with higher stacking disorder around the interface between the nucleation layer and substrate. On the other hand, the increased AlN buffer thickness gives rise to relatively higher dislocation densities. This result indicates that the restriction of propagation or generation of dislocations in GaN is possible by inserting a relatively thinner AlN buffer layer on sapphire.

One of the most serious obstacles limiting the device performance is the poor surface and interface quality of the HEMT samples. In order to elucidate the morphologic structure of the samples, AFM images of the GaN caps were taken with the scans of $5\ \mu m \times 5\ \mu m$ and $2\ \mu m \times 2\ \mu m$ scales on the samples (Fig. 4). The most distinctive feature of both samples is to have a step-flow morphology characterized by steps and terraces on the GaN surfaces, which is the same as that observed for the GaN surfaces of MOCVD-grown AlGaN/GaN HEMTs. However, a spiral step-terrace feature clustered in the form of hillocks on the surface of sample A is present, as opposed to a random step-terrace structure of sample B. The scans of $4\,\mu m^2$ enable insight into on the surface properties of the samples. The dark spots on the images are assigned to the screw component of dislocations in the GaN layers[25] in which steps are terminated. The densities of the dark spots for samples A and B were estimated as 4.0×10^8 cm^{-2} and 8.3×10^8 cm^{-2} by counting the dark spots on their images of $4\,\mu m^2$. The dark spot density of sample B is approximately twice higher than that of sample A. The dislocation reduction with screw character is related to the spiral step-terrace structure on the surface of sample A, which is in agreement with a report by Bai et al.[26] AFM (in excess of 10^7 cm^{-2}) overestimates the screw dislocation density of the samples by computed from the (0002) peaks. The discrepancy between the two results is presumably due to the small scan area of AFM, and then again, in addition to the dislocations in an epitaxial film the grain size and microstrain make a contribution to broadening of the x-ray reflections.[27]

The surface roughness of the AlInN-barrier structures was evaluated via the root-mean-square (rms) parameter, which is the root mean square of difference between the surface height and average height.[28] The rms values of samples A and B, as measured over a scan of $5\ \mu m \times 5\ \mu m$, are 0.30 nm and 0.46 nm. While the rms roughness of sample A is comparable with one monolayer of GaN indicating to a flat surface, the rms of sample B is corresponding to one-two layers. The surface rms roughness shows an increase with respect to the buffer thickness. The rough surface of sample B compared to sample A is on account of its different step-terrace structure and the larger dark spot density. Obviously, AFM analysis indicates that the relatively thinner buffer leads to an observable improvement in the surface quality of the heterostructures, which is consistent with the structural perfection as evidenced from the XRD measurements.

X-ray reflectivity (XRR) is a useful technique for determining the interface quality of layers in a heterostructure. Figure 5 shows XRR curves for samples A and B in an angular interval of 0°–6°. There appear strong periodic oscillations for each structure, so-called Kiessig fringes. The presence of the fringes reveals that the samples have a good interfacial quality. The amplitude and frequency of the oscillations are affected by thicknesses of layers in a heterostructure, differences in the densities of the layers, and the interface roughness of the structure.[19] The thickness of the AlInN barrier

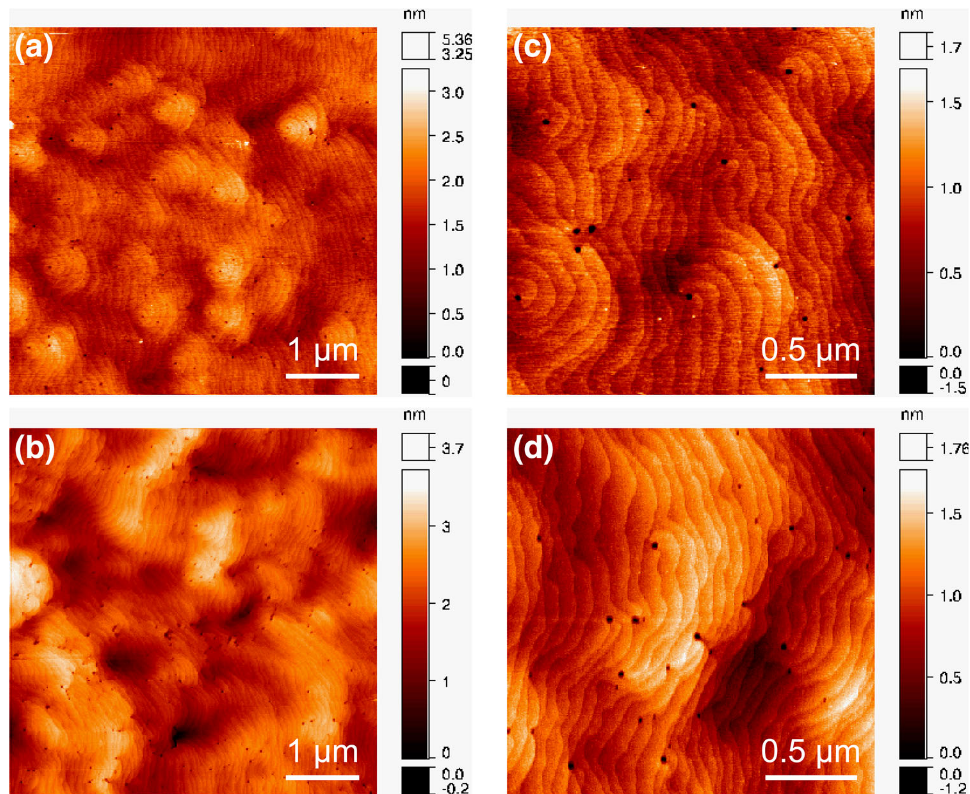

Fig. 4. (Color online) AFM images with 5 μm × 5 μm and 2 μm × 2 μm scan area of AlInN-barrier HEMT structures showing step-terraces features: (a, c) for sample A and (b, d) for sample B.

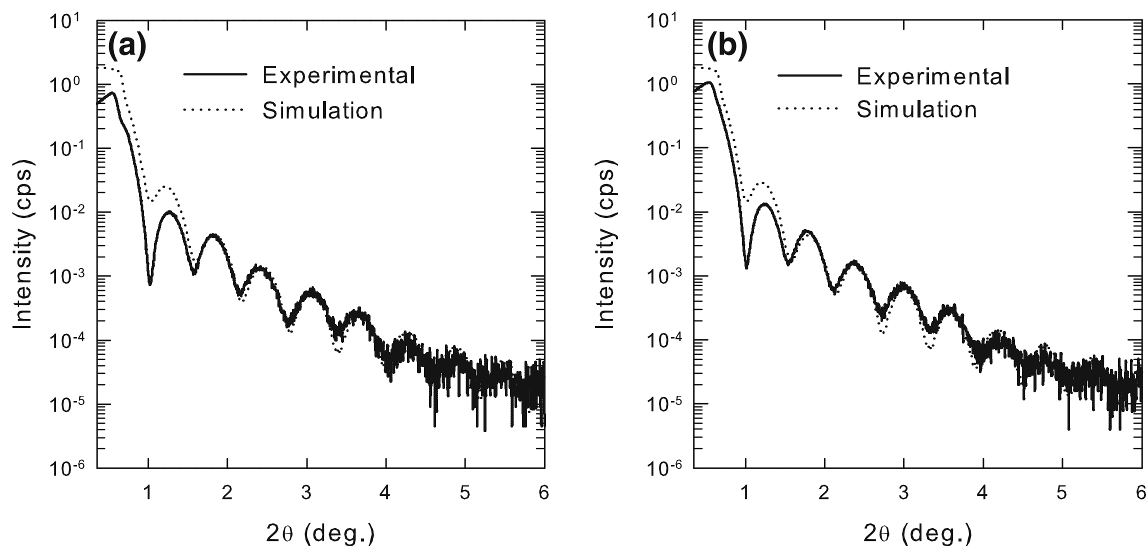

Fig. 5. Specular x-ray reflectivity of samples (a) and (b) with fitted curves.

layers and the roughness in their upper surface were estimated as 5.2 nm and 0.82 nm for sample A and 4.9 nm and 1.72 nm for sample B from simulation of the nominal structure by fitting the XRR curves. This result indicates that sample A with the thinner buffer layer has a better interface quality between GaN cap layer and AlInN barrier layer.

Figure 6 plots the room-temperature PL spectra for the AlN-buffered structures. The spectra exhibit a sharp and intense nearly band edge (BE) emission at about 369 nm, a blue emission at about 437 nm, a yellow emission at about 550 nm, and another weak emission at about 735 nm. The blue luminescence (BL) band is characteristic for MOCVD-grown GaN

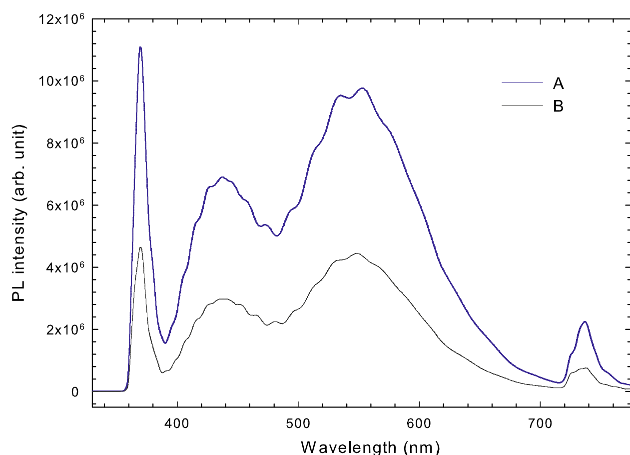

Fig. 6. (Color online) Room-temperature PL spectra of the samples with different AlN buffer thicknesses.

films[29] and is owing to intrinsic defects that can deteriorate the crystalline quality of GaN.[30] The broad yellow luminescence (YL) band in the wavelength range of 470–700 nm and centered at ~550 nm, detected from both samples, is typical for GaN films. The origin of the YL emission is attributed to several impurities and native defects in the literature and its formation mechanism is a subject of debate. A number of studies on the origin and formation mechanism of the BL and YL bands have been presented in our previous report.[31] In general, the ratio of the BE peak intensity to the YL peak intensity (*BE/YL*) is used as a criterion for film quality.[32–34] The *BE/YL* peak intensity ratios were estimated as 1.12 and 1.04 for samples A and B, respectively. The present PL results are compatible with the enhancement in the structural quality of sample A, as verified by XRD and AFM analyzes.

The two-dimensional electron gas transport properties of the AlInN-barrier structures were investigated via the Hall-effect measurements. The measurements were performed using van der Pauw geometry at room-temperature. A magnetic field of 0.57 T was applied perpendicular to the surface of the sample. The electron mobility and carrier concentration were measured as $815\,cm^2\,V^{-1}\,s^{-1}$, $3.9 \times 10^{13}\,cm^{-2}$ for sample A and $810\,cm^2\,V^{-1}\,s^{-1}$, $3.6 \times 10^{13}\,cm^{-2}$ for sample B, which resulted in sheet resistances of $196\,\Omega\,sq^{-1}$ and $214\,\Omega\,sq^{-1}$, respectively. These results are consistent with AFM observations and XRD results, and indicate that samples in this study are feasible for the device applications. When viewed as a whole to the results of this study, it is clear that the growth of the thinner AlN buffer on sapphire enhances the structural quality of AlInN-barrier heterostructures. Last of all, the usage of structure with 280-nm-thick AlN buffer is favorably for HEMTs. However, the effects of buffer thickness on the interface properties of these structures and device performance require further investigation.

CONCLUSIONS

Two kinds of MOCVD-grown structures having an AlN buffer layer have been investigated by XRD, AFM, PL and Hall-effect systems. The XRD results demonstrate that a 280-nm-thick AlN buffer has a stronger capability to block propagating of dislocations into the GaN layer in the structure. The AFM results exhibit that the lower buffer thickness leads to a reduction of the dark spot density on the surface and a smooth surface. The PL results and Hall data for the AlInN/AlN/GaN structure with the thin buffer are compatible with the improvement in its structural quality. To conclude, further efforts are needed to optimize the novel AlInN-barrier structures to realize high-performance HEMTs.

ACKNOWLEDGEMENTS

This work is supported by the Ministry of Development of TR under Project No: 2011K120290. This work is also supported by Kırklareli University (KLÜBAP/053).

REFERENCES

1. Y.-F. Wu, D. Kapolnek, J.P. Ibbetson, P. Parikh, B.P. Keller, and U.K. Mishra, *IEEE Trans. Electron Devices* 48, 586 (2001).
2. H. Kim, R.M. Thompson, V. Tilak, T.R. Prunty, J.R. Shealy, and L.F. Eastman, *IEEE Electron Device Lett.* 24, 421 (2003).
3. O. Ambacher, J. Smart, J.R. Shealy, N.G. Weimann, K. Chu, and M. Murphy, *J. Appl. Phys.* 85, 3222 (1999).
4. S. Arulkumaran, T. Egawa, H. Ishikawa, and T. Jimbo, *J. Vac. Sci. Technol. B Microelectron. Nanom. Struct.* 21, 888 (2003).
5. A. Minj, D. Cavalcoli, and A. Cavallini, *Appl. Phys. Lett.* 97, 132114 (2010).
6. R. Tülek, A. Ilgaz, S. Gökden, A. Teke, M.K. Öztürk, M. Kasap, S. Özçelik, E. Arslan, and E. Özbay, *J. Appl. Phys.* 105, 1 (2009).
7. L. Shen, S. Heikman, B. Moran, R. Coffie, N. Zhang, D. Buttari, I.P. Smorchkova, S. Keller, S.P. Denbaars, and U.K. Mishra, *IEEE Electron Device Lett.* 22, 457 (2001).
8. J. Kuzmík, *IEEE Electron Device Lett.* 22, 510 (2001).
9. J. Kuzmik, A. Kostopoulos, G. Konstantinidis, J.F. Carlin, A. Georgakilas, and D. Pogany, *IEEE Trans. Electron Devices* 53, 422 (2006).
10. M. Gonschorek, J.-F. Carlin, E. Feltin, M.A. Py, N. Grandjean, V. Darakchieva, B. Monemar, M. Lorenz, and G. Ramm, *J. Appl. Phys.* 103, 093714 (2008).
11. H. Yu, M. Ozturk, P. Demirel, H. Cakmak, B. Bolukbas, D. Caliskan, and E. Ozbay, *Semicond. Sci. Technol.* 26, 085010 (2011).
12. D. Godwinraj, H. Pardeshi, S.K. Pati, N. Mohankumar, and C.K. Sarkar, *Superlattices Microstruct.* 54, 188 (2013).
13. R. Tülek, E. Arslan, A. Bayraklı, S. Turhan, S. Gökden, Ö. Duygulu, A.A. Kaya, T. Fırat, A. Teke, and E. Özbay, *Thin Solid Films* 551, 146 (2014).
14. I. Saidi, H. Mejri, M. Baira, and H. Maaref, *Superlattices Microstruct.* 84, 113 (2015).
15. T. Palacios, A. Chakraborty, S. Heikman, S. Keller, S.P. DenBaars, and U.K. Mishra, *IEEE Electron Device Lett.* 27, 13 (2006).

16. H. Kim-Chauveau, P. de Mierry, J.-M. Chauveau, and J.-Y. Duboz, *J. Cryst. Growth* 316, 30 (2011).
17. Y. Sakai, P.C. Khai, J. Ichikawa, T. Egawa, and T. Jimbo, *J. Appl. Phys.* 109, 033512 (2011).
18. A. Minj, D. Cavalcoli, G.R. Mutta Popuri, A. Vilalta-Clemente, P. Ruterana, and A. Cavallini, *Acta Mater*. 89, 290 (2015).
19. S. Çörekçi, M.K. Öztürk, B. Akaoğlu, M. Çakmak, S. Özçelik, and E. Özbay, *J. Appl. Phys*. 101, 123502 (2007).
20. S. Çörekçi, M.K. Öztürk, M. Çakmak, S. Özçelik, and E. Özbay, *Mater. Sci. Semicond. Process.* 15, 32 (2012).
21. J. Bai, T. Wang, P.J. Parbrook, K.B. Lee, and A.G. Cullis, *J. Cryst. Growth* 282, 290 (2005).
22. N. Faleev, C. Honsberg, O. Jani, and I. Ferguson, *J. Cryst. Growth* 300, 246 (2007).
23. P. Gay, P. Hirsch, and A. Kelly, *Acta Metall.* 1, 315 (1953).
24. T. Ide, M. Shimizu, X.Q. Shen, K. Jeganathan, H. Okumura, and T. Nemoto, *J. Cryst. Growth* 245, 15 (2002).
25. F.C. Frank, *Discuss. Faraday Soc.* 5, 67 (1949).
26. J. Bai, M. Dudley, W.H. Sun, H.M. Wang, and M.A. Khan, *Appl. Phys. Lett.* 88, 1 (2006).
27. H. Jiang, T. Egawa, M. Hao, and Y. Liu, *Appl. Phys. Lett.* 87, 241911 (2005).
28. K. Vanormelingen, B. Degroote, and A. Vantomme, *J. Vac. Sci. Technol. B Microelectron. Nanom. Struct.* 24, 725 (2006).
29. T. Sasaki and S. Zembutsu, *J. Appl. Phys.* 61, 2533 (1987).
30. S.T. Li, F.Y. Jiang, G.F. Han, L. Wang, C.B. Xiong, X.X. Peng, and H.L. Mo, *Mater. Sci. Eng. B-Solid State Mater. Adv. Technol*. 122, 72 (2005).
31. S. Çörekçi, M.K. Öztürk, A. Bengi, M. Çakmak, S. Özçelik, and E. Özbay, *J. Mater. Sci.* 46, 1606 (2010).
32. I. Shalish, L. Kronik, G. Segal, Y. Rosenwaks, Y. Shapira, U. Tisch, and J. Salzman, *Phys. Rev. B* 59, 9748 (1999).
33. X. Li and J.J. Coleman, *Appl. Phys. Lett.* 70, 438 (1997).
34. B. Potì, M.A. Tagliente, and A. Passaseo, *J. Non. Cryst. Solids* 352, 2332 (2006).